Flavor changing neutrino interactions and CP violation in neutrino oscillations

Toshihiko Hattori,[a),1] Tsutom Hasuike,[b),2] and Seiichi Wakaizumi[c),3]

[a)] *Institute of Theoretical Physics, University of Tokushima, Tokushima 770-8502, Japan*

[b)] *Department of Physics, Anan College of Technology, Anan 774-0017, Japan*

[c)] *Center for University Extension, University of Tokushima, Tokushima 770-8502, Japan*

Abstract

We investigate the interference effects of non-standard neutrino matter interactions (NSNI) with the mass-induced neutrino oscillations. The NSNI is composed of flavor-changing neutrino interactions (FCNI) and flavor-diagonal neutrino interactions (FDNI). Both of the interactions are introduced in the $\nu_\mu - \nu_\tau$ sector and the $\nu_e - \nu_\mu$ sector in order to study their effects in $\nu_\mu \to \nu_\tau$ and $\nu_\mu \to \nu_e$ oscillations, respectively. The FCNI effect proves to possibly dominate the CP violating effect, *i.e.* the difference between the neutrino and the antineutrino oscillation probabilities. The FCNI effect significantly survives as a fake CP violating effect in the neutrino energy region where the pure CP violating effect, ordinary matter effect and FDNI effect die out, for example, above 4 GeV at the baseline of $L = 730$ km in the $\nu_\mu \to \nu_\tau$ oscillation for the maximum parameter values of FCNI and FDNI allowed by the atmospheric neutrino oscillation data. The FCNI effect also dominates the CP violating effect in the $\nu_\mu \to \nu_e$ oscillation above 1 GeV at the baseline of $L = 300$ km for the maximum phase of FCNI.

[1]e-mail: hattori@ias.tokushima-u.ac.jp
[2]e-mail: hasuike@anan-nct.ac.jp
[3]e-mail: wakaizum@cue.tokushima-u.ac.jp

I Introduction

In the framework of massive neutrinos and leptonic mixing, the atmospheric neutrino anomaly [1] is resolved by the $\nu_\mu \to \nu_\tau$ oscillation with nearly maximal mixing between ν_μ and ν_τ [2] and the solar neutrino deficit [3] is interpreted by the $\nu_e \to \nu_\mu$ oscillation with large mixing angle [4] in the Mikheyev-Smirnov-Wolfenstein (MSW) mechanism of neutrino interactions with matter [5] in the three-neutrino scheme, where the neutrino flavor eigenstates ν_α ($\alpha = e, \mu, \tau$) are expressed by a superposition of their mass eigenstates ν_i ($i = 1, 2, 3$) with mass m_i as follows:

$$\nu_\alpha = \sum_{i=1}^{3} U_{\alpha i}\, \nu_i, \tag{1}$$

where U is the 3×3 unitary mixing matrix, which is called as Maki-Nakagawa-Sakata (MNS) matrix [6]. The reactor experiment of search for $\bar{\nu_e}$ oscillations, CHOOZ, gives an upper limit on the element U_{e3}, which is very small as $|U_{e3}| < 0.22$ [7]. The liquid scintillation experiment, LSND, claims a discovery of $\bar{\nu_\mu} \to \bar{\nu_e}$ oscillations [8], which requires a fourth sterile neutrino.

The above situation seems to convince us of a scheme of massive neutrinos and lepton mixing. In addition to this scheme, it is interesting to investigate non-standard neutrino matter interactions in the neutrino oscillations. The non-standard neutrino matter interaction (NSNI) is originated from Wolfenstein's work [9] and then was studied in order to solve the solar neutrino deficit [10]. In 1999, the flavor-changing neutrino matter interaction (FCNI) is applied to account for the observed zenith-angle-dependent deficit of atmospheric neutrinos [11]. And then, FCNI and flavor-diagonal neutrino matter interaction (FDNI) are used to consider the total rate, day-night and seasonal variations of the event rate and the recoil electron energy spectrum measured by the solar neutrino experiments [12]. The mere FCNI, however, has proved not to be able to solve the atmospheric neutrino problem [13]. After that, the FCNI is studied as sub-leading effects to the

standard mass-induced neutrino oscillations by considering FCNI in $\nu_\mu - \nu_\tau$ sector and in $\nu_e - \nu_\tau$ sector [13][14] and its detectability at a future neutrino factory is discussed in Refs.[14][15]. There are also combined analyses with the inclusion of new flavor-changing neutrino interactions occuring in the neutrino production and detection processes in addition to the above-mentioned FCNI, of which effects are enhanced by the interference with the ordinary weak interactions in the oscillation phenomena [16] [17].

In this paper, we analyze the non-standard neutrino matter interaction effects (NSNI) to the CP violating effects in the neutrino oscillations by considering them in $\nu_\mu - \nu_\tau$ sector and $\nu_e - \nu_\mu$ sector in the three-neutrino scheme. The NSNI consists of the above-mentioned FCNI and flavor-diagonal neutrino matter interactions (FDNI). The evolution equation of the neutrino flavor states is solved analytically by using Arafune-Koike-Sato's perturbative method [18] and we calculate the neutrino oscillation probability for the general $\nu_\alpha \to \nu_\beta$ oscillation. We apply this analytic expression of the probability to calculate the CP violating effects in $\nu_\mu \to \nu_\tau$ and $\nu_\mu \to \nu_e$ oscillations, *i.e.* the difference between the neutrino and the antineutrino oscillation probabilities. We find that the FCNI matter effect survives and dominates the CP violating effects even after both the pure CP violating effect due to the phase of U and the fake CP violating ones due to the ordinary and FDNI matter effects die out. This shows that the non-standard flavor changing neutrino matter interaction could be detected in the CP violating effect in neutrino oscillations at the neutrino energies where both the pure CP violating effect and the ordinary matter effect become sufficiently small and undetectable.

The paper is organized as follows. In Sec. II the oscillation probability is derived by solving analytically the evolution equation of the neutrino flavor states with the non-standard neutrino matter interaction in $\nu_\mu - \nu_\tau$ sector. The effect of the NSNI is studied in the CP violating effects in the $\nu_\mu \to \nu_\tau$ oscillation. In

Sect. III the same will be done for the NSNI in $\nu_e - \nu_\mu$ sector and the effect of the NSNI is studied in the CP violating effects in the $\nu_\mu \to \nu_e$ oscillation. Section IV is devoted to the conclusions and discussions.

II Oscillation probability and CP violating effect with NSNI in $\nu_\mu - \nu_\tau$ sector

Here and in the next section we calculate the neutrino oscillation probabilities and CP violating effects with the inclusion of the NSNI in $\nu_\mu - \nu_\tau$ sector and in $\nu_e - \nu_\mu$ sector, respectively, in the three-neutrino scheme by solving analylitically the evolution equation for neutrino flavor states in the perturbative method.

If we consider the effect of NSNI in the $\nu_\mu - \nu_\tau$ sector, the evolution equation in matter is given as

$$i\,\frac{d}{dx}\begin{pmatrix}\nu_e\\ \nu_\mu\\ \nu_\tau\end{pmatrix} = H\begin{pmatrix}\nu_e\\ \nu_\mu\\ \nu_\tau\end{pmatrix}, \tag{2}$$

and [14]

$$H = \frac{1}{2E}U\begin{pmatrix}0 & 0 & 0\\ 0 & \Delta m^2_{21} & 0\\ 0 & 0 & \Delta m^2_{31}\end{pmatrix}U^\dagger + \begin{pmatrix}V_e(x) & 0 & 0\\ 0 & 0 & \epsilon^f_{\mu\tau}V_f(x)\\ 0 & \epsilon^{f*}_{\mu\tau}V_f(x) & \epsilon^f_{\tau\tau}V_f(x)\end{pmatrix}, \tag{3}$$

where E is the neutrino energy, $\Delta m^2_{ij} = m^2_i - m^2_j$, m_i being the mass of i-th neutrino, U is the MNS leptonic mixing matrix, $V_f(x) = \sqrt{2}G_F n_f(x)$, x being the position of the running neutrino, $\epsilon^f_{\mu\tau}V_f(x)$ is the flavor-changing $\nu_\mu + f \to \nu_\tau + f$ forward scattering amplitude due to the flavor-changing neutrino matter interaction(FCNI) and $\epsilon^f_{\tau\tau}V_f(x)$ is the flavor-diagonal $\nu_\tau - f$ elastic forward scattering amplitude due to the flavor-diagonal neutrino matter interaction(FDNI), with $n_f(x)$ being the number density of the fermion $f(f = u, d, e)$ which induces such processes. In Eq.(3), $\epsilon^f_{\mu\tau}$ and $\epsilon^f_{\tau\tau}$ are the phenomenological parameters which characterize the strength of FCNI and FDNI, respectively. The fermion number density $n_f(x)$ can be written in terms of the matter density ρ as $n_f(x) = \rho(x)Y_f$,

where Y_f is the fraction of the fermion f per nucleon, $\sim 1/2$ for electrons and $\sim 3/2$ for u or d quarks.

For the evolution equation of the antineutrinos, the replacement of $U \to U^*, V_{e,f}(x) \to -V_{e,f}(x)$ and $\epsilon^f_{\mu\tau} \to \epsilon^{f*}_{\mu\tau}$ should be done in Eq.(3).

We use here Arafune-Koike-Sato's perturbative method to solve analytically the evolution equation [18]. The solution of Eq.(2) is given by

$$\nu(x) = S(x)\nu(0), \tag{4}$$

with

$$S(x) = T\exp\left(-i\int_0^x dsH(s)\right), \tag{5}$$

where

$$\nu(x) = \begin{pmatrix} \nu_e(x) \\ \nu_\mu(x) \\ \nu_\tau(x) \end{pmatrix} \tag{6}$$

and T is the time ordering operator. In the following, the oscillation probability and the CP violating effect are calculated for the baseline of $L = 300$ and 730 km so that we assume $n_f(x)$ and $\rho(x)$ to be independent of x. Then we have

$$S(x) = e^{-i\,Hx}. \tag{7}$$

The oscillation probability for $\nu_\alpha \to \nu_\beta$ at the distance L from the neutrino production point is given in terms of S in Eq.(5) as follows:

$$P(\nu_\alpha \to \nu_\beta; L) = \left|S_{\beta\alpha}(L)\right|^2. \tag{8}$$

We express the Hamiltonian H of Eq.(3) for simplicity as

$$H = \frac{1}{2E}U\begin{pmatrix} 0 & 0 & 0 \\ 0 & \Delta m^2_{21} & 0 \\ 0 & 0 & \Delta m^2_{31} \end{pmatrix}U^\dagger + \frac{1}{2E}\begin{pmatrix} a & 0 & 0 \\ 0 & 0 & \epsilon b \\ 0 & \epsilon^* b & \epsilon' b \end{pmatrix}, \tag{9}$$

where

$$a \equiv 2EV_e = 2\sqrt{2}G_F n_e E = 7.60\times 10^{-5}\frac{\rho}{[\mathrm{g\,cm^{-3}}]}\frac{E}{[\mathrm{GeV}]}\ \mathrm{eV}^2, \tag{10}$$

$$\epsilon b \equiv 2E\epsilon^f_{\mu\tau}V_f = 15.2\times 10^{-5}\epsilon Y_f \frac{\rho}{[\mathrm{g\,cm^{-3}}]}\frac{E}{[\mathrm{GeV}]}\ \mathrm{eV}^2, \tag{11}$$

$$\epsilon' b \equiv 2E\epsilon^f_{\tau\tau}V_f = 15.2\times 10^{-5}\epsilon' Y_f \frac{\rho}{[\mathrm{g\,cm^{-3}}]}\frac{E}{[\mathrm{GeV}]}\ \mathrm{eV}^2, \tag{12}$$

where $\epsilon^f_{\mu\tau}$ and $\epsilon^f_{\tau\tau}$ are denoted as ϵ and ϵ', respectively, and V_f is denoted as b, for simplicity. In general, ϵ is complex and ϵ' is real from the hermeticity of the Hamiltonian. Since $\Delta m^2_{21} \ll \Delta m^2_{31}$ and $a, |\epsilon|b, |\epsilon'|b \ll \Delta m^2_{31}$ because of $|\epsilon| < 0.04$ and $|\epsilon'| < 0.17$ from the analysis of the atmospheric neutrino problem [13], we decompose H of Eq.(9) as $H = H_0 + H_1$ with

$$H_0 = \frac{1}{2E}U\begin{pmatrix} 0 & 0 & 0 \\ 0 & 0 & 0 \\ 0 & 0 & \Delta m^2_{31}\end{pmatrix}U^\dagger, \tag{13}$$

and

$$H_1 = \frac{1}{2E}U\begin{pmatrix} 0 & 0 & 0 \\ 0 & \Delta m^2_{21} & 0 \\ 0 & 0 & 0\end{pmatrix}U^\dagger + \frac{1}{2E}\begin{pmatrix} a & 0 & 0 \\ 0 & 0 & \epsilon b \\ 0 & \epsilon^* b & \epsilon' b\end{pmatrix}, \tag{14}$$

and treat H_1 as a perturbation and calculate Eq.(7) up to the first order in $\Delta m^2_{21}, a, \epsilon b$ and $\epsilon' b$. Then, $S(x)$ is given by

$$S(x) \simeq e^{-i\,H_0 x} - i\,e^{-i\,H_0 x}\int_0^x ds H_1(s), \tag{15}$$

where $H_1(x) = e^{i\,H_0 x}H_1\,e^{-i\,H_0 x}$. The approximation in Eq.(15) requires

$$\frac{\Delta m^2_{21}L}{2E} \ll 1, \qquad \frac{|\epsilon|bL}{2E} \ll 1, \qquad \frac{\epsilon' bL}{2E} \ll 1. \tag{16}$$

The requirements of Eq.(16) are satisfied for $\Delta m^2_{21} = (10^{-5}-10^{-4})\ \mathrm{eV}^2, E = 1-20$ GeV, $L = (300-730)$ km, $\rho = 3\mathrm{g/cm}^3, |\epsilon| \sim 0.03$ and $|\epsilon'| \sim 0.16$ as

$$\begin{aligned} \frac{\Delta m^2_{21}L}{2E} &\simeq 4\times 10^{-4} - 0.2, \qquad \frac{|\epsilon|bL}{2E} \simeq (1-4)\times 10^{-2}, \\ \frac{|\epsilon'|bL}{2E} &\simeq (1-2)\times 10^{-1}. \end{aligned} \tag{17}$$

Equation (16) also shows that the approximation becomes better as the energy E increases. If we express $S_{\beta\alpha}(x)$ as

$$S_{\beta\alpha}(x) = \delta_{\beta\alpha} + i\,T_{\beta\alpha}(x), \tag{18}$$

then $i\,T_{\beta\alpha}(x)$ is obtained as follows:

$$
\begin{aligned}
i\,T_{\beta\alpha}(x) \;=\; & -2\,i\exp\left(-i\,\frac{\Delta m^2_{31}x}{4E}\right)\sin\left(\frac{\Delta m^2_{31}x}{4E}\right)\Big[\,U_{\beta3}U^*_{\alpha3}\{1-\frac{a}{\Delta m^2_{31}}(2|U_{e3}|^2 \\
& -\delta_{\alpha e}-\delta_{\beta e})-i\,\frac{ax}{2E}|U_{e3}|^2-\frac{\epsilon' b}{\Delta m^2_{31}}(2|U_{\tau3}|^2-\delta_{\alpha\tau}-\delta_{\beta\tau}) \\
& -i\,\frac{\epsilon' bx}{2E}|U_{\tau3}|^2\}-\frac{1}{\Delta m^2_{31}}\{4U^*_{\alpha3}U_{\beta3}\mathrm{Re}(\epsilon bU^*_{\mu3}U_{\tau3}) \\
& -\epsilon^* b(U^*_{\alpha3}U_{\mu3}\delta_{\beta\tau}+U_{\beta3}U^*_{\tau3}\delta_{\alpha\mu})-\epsilon b(U^*_{\alpha3}U_{\tau3}\delta_{\beta\mu} \\
& +U_{\beta3}U^*_{\mu3}\delta_{\alpha\tau})\}-2\,i\,\frac{x}{2E}U^*_{\alpha3}U_{\beta3}\mathrm{Re}(\epsilon bU^*_{\mu3}U_{\tau3})\,\Big] \\
& -i\,\frac{\Delta m^2_{31}x}{2E}\Big[\,\frac{\Delta m^2_{21}}{\Delta m^2_{31}}U_{\beta2}U^*_{\alpha2}+\frac{a}{\Delta m^2_{31}}\{\delta_{\alpha e}\delta_{\beta e}+U_{\beta3}U^*_{\alpha3}(2|U_{e3}|^2-\delta_{\alpha e} \\
& -\delta_{\beta e})\}+\frac{\epsilon' b}{\Delta m^2_{31}}\{\delta_{\alpha\tau}\delta_{\beta\tau}+U_{\beta3}U^*_{\alpha3}(2|U_{\tau3}|^2-\delta_{\alpha\tau}-\delta_{\beta\tau})\} \\
& +\frac{1}{\Delta m^2_{31}}\{\epsilon^* b\delta_{\beta\tau}\delta_{\alpha\mu}+\epsilon b\delta_{\beta\mu}\delta_{\alpha\tau}+4U^*_{\alpha3}U_{\beta3}\mathrm{Re}(\epsilon bU^*_{\mu3}U_{\tau3}) \\
& -\epsilon^* b(U^*_{\alpha3}U_{\mu3}\delta_{\beta\tau}+U_{\beta3}U^*_{\tau3}\delta_{\alpha\mu})-\epsilon b(U^*_{\alpha3}U_{\tau3}\delta_{\beta\mu} \\
& +U_{\beta3}U^*_{\mu3}\delta_{\alpha\tau})\}\,\Big]. \qquad (19)
\end{aligned}
$$

We use Eq.(19) in Eq.(18) and calculate the oscillation probability for $\nu_\alpha \to \nu_\beta$ by Eq.(8). The complete expression of $P(\nu_\alpha \to \nu_\beta; L)$ with the NSNI in $\nu_\mu - \nu_\tau$ sector is given in the Appendix A.

Now we will study the effects due to the NSNI in $\nu_\mu - \nu_\tau$ sector on the oscillation probability and the CP violating effect in $\nu_\mu \to \nu_\tau$ oscillation at the baseline of $L = 730$ km. For the MNS mixing matrix U, we take the standard parametrization given by

$$
U = \begin{pmatrix} c_{12}c_{13} & s_{12}c_{13} & s_{13}e^{-i\,\delta} \\ -s_{12}c_{23}-c_{12}s_{23}s_{13}e^{i\,\delta} & c_{12}c_{23}-s_{12}s_{23}s_{13}e^{i\,\delta} & s_{23}c_{13} \\ s_{12}s_{23}-c_{12}c_{23}s_{13}e^{i\,\delta} & -c_{12}s_{23}-s_{12}c_{23}s_{13}e^{i\,\delta} & c_{23}c_{13} \end{pmatrix}, \qquad (20)
$$

where $c_{ij} = \cos\theta_{ij}, s_{ij} = \sin\theta_{ij}$ and δ is the CP violating phase. From the Super-Kamiokande data for the atmospheric neutrino oscillation [2], $\sin^2 2\theta_{\rm atm} > 0.82$ and $5\times10^{-4} < \Delta m^2_{\rm atm} < 6\times10^{-3}$ eV^2, we take in the following $\sin\theta_{23} = 0.742$ for the mixing angle s_{23} and $\Delta m^2_{31} = 2.5\times10^{-3}$ eV^2 as a typical value. For s_{12}, we

take $\sin\theta_{12} = 0.541$ and $\Delta m^2_{21} = 5 \times 10^{-5}$ eV^2 from the presently most probable large-mixing angle solution (LMA) to the solar neutrino oscillation [19]. For s_{13}, we tentatively assume $\sin\theta_{13} = 0.16$ from the CHOOZ data on $\bar{\nu_e}$ oscillation [7], $\sin^2 2\theta_{\rm CHOOZ} < 0.18$ for $3 \times 10^{-3} < \Delta m^2 < 1.0 \times 10^{-2}$ eV^2, which means $0 < \sin\theta_{13} < 0.22$. For the phenomenological parameters of the NSNI, the constraints are derived to be $-0.05 < \epsilon < 0.04$ and $|\epsilon'| < 0.17$ from the analyses of the atmospheric neutrino data by Fonengo et al. [13]. They assumed ϵ to be real. Here we generally take ϵ to be complex. For the numerical calculations we take $|\epsilon| = 0.03$ and $\epsilon' = \pm 0.16$, and the effects of the FCNI on CP violation has proved to be maximum at $\phi = 0$ and π for the phase of ϵ, $\epsilon = |\epsilon|\, e^{i\phi}$.

In the following, we present the numerical results for the oscillation probabilities and CP violating effects in the $\nu_\mu \to \nu_\tau$ oscillation. The effect of NSNI in the $\nu_\mu - \nu_\tau$ sector is not so significant in the $\nu_\mu \to \nu_e$ and $\nu_e \to \nu_\tau$ oscillations as in the $\nu_\mu \to \nu_\tau$ oscillation. Fig.1 and Fig.2 show the $\nu_\mu \to \nu_\tau$ oscillation probabilities for $|\epsilon| = 0.03, \phi = 0, \epsilon' = 0.16, \delta = \pi/2, \Delta m^2_{31} > 0$ for the neutrino energy range of $E = 0.1 - 1$ GeV and $E = 1 - 20$ GeV, respectively, at the baseline of $L = 730$ km, where the solid line represents the oscillation probability including all the three matter effects, *i.e.* ordinary matter effect (denoted as a in Eq.(14)), flavor-changing neutrino matter interaction (FCNI, denoted as ϵb) and flavor-diagonal neutrino matter interaction (FDNI, denoted as $\epsilon' b$), and the dashed line represents the one without any matter effects. Fig.3 shows the oscillation probabilities for $\phi = \pi$ with the same values of $|\epsilon|$ and ϵ' as in Figs.1 and 2. These three Figures show that the matter effects due to the NSNI are small on the oscillation probability.

Figs.4-9 show the CP violating effects in the $\nu_\mu \to \nu_\tau$ oscillation, calculated as the difference between the neutrino and the antineutrino oscillation probabilities, for the energy range of $E = 1 - 20$ GeV at the baseline of $L = 730$ km. The phase

of the MNS mixing matrix U is taken as $\delta = \pi/2$. The dash-dotted line is the pure CP violating effect due to the phase of U. The long-dashed, short-dashed and dotted lines are the fake CP violating efects due to the ordinary, FCNI and FDNI matter effects, respectively. The solid line represents the total CP violating effect with the sum of the pure and fake ones. In Figs.6-8, the FDNI contribution is not drawn, since it is of the same magnitude as in Figs.4-5 apart from its sign. For Figs.4-8, we have taken $|\epsilon| = 0.03, |\epsilon'| = 0.16$ and $|\Delta m^2_{31}| = 2.5 \times 10^{-3}$ eV^2. In Fig.4, the phase of ϵ is taken as $\phi = 0$ and $\epsilon' = +0.16$ (> 0) and $\Delta m^2_{31} > 0$. In Fig.5, $\phi = 0, \epsilon' = -0.16$ (< 0) and $\Delta m^2_{31} > 0$. In Fig.6, $\phi = \pi, \epsilon' > 0$ and $\Delta m^2_{31} > 0$. In Fig.7, $\phi = 0, \epsilon' > 0$ and $\Delta m^2_{31} < 0$ and in Fig.8, $\phi = \pi, \epsilon' > 0$ and $\Delta m^2_{31} < 0$. As can be seen from these Figures, the FCNI matter effect dominates the CP violating effect in the whole range of $E = 1 - 20$ GeV, and all the other contributions of pure CP violation, ordinary matter effect and FDNI effect rapidly die out around 4 GeV and the FCNI effect survives significantly above this energy. When the sign of Δm^2_{31} is changed, the contributions of all the matter effects including FCNI and FDNI change the sign, as can be seen from the comparison of Fig.4 and Fig.7. In Fig.9 the pure and fake CP violating effects are shown for the smaller ϵ and ϵ' values, $|\epsilon| = 0.01, \phi = 0$ and $\epsilon' = 0.01$.

III NSNI in $\nu_e - \nu_\mu$ sector

In this section, we consider the NSNI in $\nu_e - \nu_\mu$ sector and study its effect on the oscillation probability and CP violating effect in $\nu_\mu \to \nu_e$ oscillation at the baselines of $L = 300$ and 730 km.

The Hamiltonian of the evolution equation of the flavor neutrino states is given as

$$H = \frac{1}{2E} U \begin{pmatrix} 0 & 0 & 0 \\ 0 & \Delta m^2_{21} & 0 \\ 0 & 0 & \Delta m^2_{31} \end{pmatrix} U^\dagger + \begin{pmatrix} V_e(x) & \epsilon^f_{e\mu} V_f(x) & 0 \\ \epsilon^{f*}_{e\mu} V_f(x) & \epsilon^f_{\mu\mu} V_f(x) & 0 \\ 0 & 0 & 0 \end{pmatrix}, \qquad (21)$$

where $\epsilon^f_{e\mu} V_f(x)$ is the flavor-changing $\nu_e + f \to \nu_\mu + f$ forward scattering ampli-

tude due to the FCNI and $\epsilon^f_{\mu\mu}V_f(x)$ is the flavor-diagonal $\nu_\mu - f$ elastic forward scattering amplitude due to the FDNI. As in the previous section, we assume the matter density to be constant for the baseline of $L = 300$ and 730 km and reexpress Eq.(21) as

$$H = \frac{1}{2E}U\begin{pmatrix}0 & 0 & 0\\ 0 & \Delta m^2_{21} & 0\\ 0 & 0 & \Delta m^2_{31}\end{pmatrix}U^\dagger + \frac{1}{2E}\begin{pmatrix}a & \eta b & 0\\ \eta^* b & \eta' b & 0\\ 0 & 0 & 0\end{pmatrix}, \tag{22}$$

where a is the same as in Eq.(10) and

$$\eta b \equiv 2E\epsilon^f_{e\mu}V_f = 15.2\times 10^{-5}\eta Y_f \frac{\rho}{[\mathrm{g\,cm^{-3}}]}\frac{E}{[\mathrm{GeV}]}\ \mathrm{eV}^2, \tag{23}$$

$$\eta' b \equiv 2E\epsilon^f_{\mu\mu}V_f = 15.2\times 10^{-5}\eta' Y_f \frac{\rho}{[\mathrm{g\,cm^{-3}}]}\frac{E}{[\mathrm{GeV}]}\ \mathrm{eV}^2, \tag{24}$$

where $\epsilon^f_{e\mu}$ and $\epsilon^f_{\mu\mu}$ are denoted as η and η', respectively, and V_f is denoted as b, for simplicity. In general, η is complex and η' is real and their magnitudes are expected to be much smaller than 1 in the same way as for ϵ and ϵ' in the $\nu_\mu - \nu_\tau$ sector. The phenomenological constraint on η and η' does not exist, although they will be estimated from $\nu_\mu \to \nu_e$ oscillation. So, we decompose H of Eq.(22) as $H = H_0 + H_1$ with

$$H_1 = \frac{1}{2E}U\begin{pmatrix}0 & 0 & 0\\ 0 & \Delta m^2_{21} & 0\\ 0 & 0 & 0\end{pmatrix}U^\dagger + \frac{1}{2E}\begin{pmatrix}a & \eta b & 0\\ \eta^* b & \eta' b & 0\\ 0 & 0 & 0\end{pmatrix}, \tag{25}$$

and treat H_1 as a perturbation. H_0 is the same as in Eq.(13). In the same way as for the NSNI in $\nu_\mu - \nu_\tau$ sector, we calculate $S(x)$ of Eq.(7) up to the first order in $\Delta m^2_{21}, a, \eta b$ and $\eta' b$ to obtain the expression of $i\,T_{\beta\alpha}(x)$ in Eq.(18):

$$\begin{aligned} i\,T_{\beta\alpha}(x) = & -2\,i\exp\left(-i\,\frac{\Delta m^2_{31}x}{4E}\right)\sin\left(\frac{\Delta m^2_{31}x}{4E}\right)\Big[\,U_{\beta 3}U^*_{\alpha 3}\{1 - \frac{a}{\Delta m^2_{31}}(2|U_{e3}|^2 \\ & - \delta_{\alpha e} - \delta_{\beta e}) - i\,\frac{ax}{2E}|U_{e3}|^2 - \frac{\eta' b}{\Delta m^2_{31}}(2|U_{\mu 3}|^2 - \delta_{\alpha\mu} - \delta_{\beta\mu}) \\ & - i\,\frac{\eta' bx}{2E}|U_{\mu 3}|^2\} - \frac{1}{\Delta m^2_{31}}\{4U^*_{\alpha 3}U_{\beta 3}\mathrm{Re}(\eta b U^*_{e3}U_{\mu 3}) \\ & - \eta^* b(U^*_{\alpha 3}U_{e3}\delta_{\beta\mu} + U_{\beta 3}U^*_{\mu 3}\delta_{\alpha e}) - \epsilon b(U^*_{\alpha 3}U_{\mu 3}\delta_{\beta e} \end{aligned}$$

$$
\begin{aligned}
&+ U_{\beta 3}U^*_{e3}\delta_{\alpha\mu})\} - 2\,i\,\frac{x}{2E}U^*_{\alpha 3}U_{\beta 3}\mathrm{Re}(\eta b U^*_{e3}U_{\mu 3})\,\Big] \\
&- i\,\frac{\Delta m^2_{31}x}{2E}\Big[\,\frac{\Delta m^2_{21}}{\Delta m^2_{31}}U_{\beta 2}U^*_{\alpha 2} + \frac{a}{\Delta m^2_{31}}\{\delta_{\alpha e}\delta_{\beta e} + U_{\beta 3}U^*_{\alpha 3}(2|U_{e3}|^2 - \delta_{\alpha e} \\
&- \delta_{\beta e})\} + \frac{\eta' b}{\Delta m\ {}_{31}^2}\{\delta_{\alpha\mu}\delta_{\beta\mu} + U_{\beta 3}U^*_{\alpha 3}(2|U_{\mu 3}|^2 - \delta_{\alpha\mu} - \delta_{\beta\mu})\} \\
&+ \frac{1}{\Delta m^2_{31}}\{\eta^* b\delta_{\beta\mu}\delta_{\alpha e} + \eta b\delta_{\beta e}\delta_{\alpha\mu} + 4U^*_{\alpha 3}U_{\beta 3}\mathrm{Re}(\eta b U^*_{e3}U_{\mu 3}) \\
&- \eta^* b(U^*_{\alpha 3}U_{e3}\delta_{\beta\mu} + U_{\beta 3}U^*_{\mu 3}\delta_{\alpha e}) - \eta b(U^*_{\alpha 3}U_{\mu 3}\delta_{\beta e} \\
&+ U_{\beta 3}U^*_{e3}\delta_{\alpha\mu})\}\,\Big]. \qquad (26)
\end{aligned}
$$

Using Eq.(26) in Eq.(18), we calculate the oscillation probability for $\nu_\alpha \to \nu_\beta$ by Eq.(8). The complete expression of $P(\nu_\alpha \to \nu_\beta; L)$ with the NSNI in $\nu_e - \nu_\mu$ sector is given in the Appendix B.

Now we will study the effects due to the NSNI in $\nu_e - \nu_\mu$ sector on the oscillation probability and the CP violating effect in $\nu_\mu \to \nu_e$ oscillation at the baselines of $L = 300$ and 730 km. The values of the parameters $\Delta m^2_{21}, \Delta m^2_{31}, s_{23}, s_{12}$ and s_{13} are taken to be the same as in the previous section. Since there are no constraints on the strength of NSNI in $\nu_e - \nu_\mu$ sector, we will take two cases of $|\eta| = |\eta'| = 0.10$ and $|\eta| = |\eta'| = 0.03$ and the effect of the FCNI on CP violation has proved to be maximum at $\gamma = \pi/2$ and $3\pi/2$ for the phase of $\eta, \eta = |\eta|\mathrm{e}^{i\,\gamma}$.

In the following, we present the numerical results for the oscillation probabilities and CP violating effects in the $\nu_\mu \to \nu_e$ oscillation. The effect of NSNI in the $\nu_e - \nu_\mu$ sector is not so significant in the $\nu_e \to \nu_\tau$ and $\nu_\mu \to \nu_\tau$ oscillations as in the $\nu_\mu \to \nu_e$ oscillation. In Fig.10 and Fig.11, we show the $\nu_\mu \to \nu_e$ oscillation probabilities for $|\eta| = 0.10, \gamma = \pi/2, \eta' = 0.10$ and for $|\eta| = 0.03, \gamma = \pi/2, \eta' = 0.03$, respectively, in the neutrino energy range of $E = 0.3 - 2$ GeV at the baseline of $L = 300$ km for $\Delta m^2_{31} > 0$ and $\delta = \pi/2$, where the solid line represents the probability with the inclusion of all the three matter effects, *i.e.* ordinary matter effect (denoted as a in Eq.(25)), flavor-changing neutrino matter interaction (FCNI, denoted as ηb) and flavor diagonal neutrino matter interaction (FDNI, de-

noted as $\eta' b$), and the dashed line represents the one without any matter effects. The case of $|\eta| = 0.10$ and $\eta' = 0.10$ (Fig.10) gives the matter effects about three times bigger than the case of $|\eta| = 0.03$ and $\eta' = 0.03$ (Fig.11) on the oscillation probability.

In Figs.12-16 we show the CP violating effects in the $\nu_\mu \to \nu_e$ oscillation, calculated as the difference between the neutrino and the antineutrino oscillatiion probabilities, for the energy range of $E = 0.3 - 2$ GeV at the baseline of $L = 300$ km (Figs.12-15) and for $E = 0.5 - 2.5$ GeV at $L = 730$ km (Fig.16). The phase of the mixing matrix U is taken as $\delta = \pi/2$. The dash-dotted line represents the pure CP violating effect due to the phase of U. The long-dashed, short-dashed and dotted lines are the fake CP violating effects due to the ordinary, FCNI and FDNI matter effects, respectively. The solid line represents the total CP violating effect, which is the sum of the pure and fake ones. The contribution of the FDNI effects is remarkably small. In Fig.12 is given the case of $|\eta| = 0.10, \eta' = 0.10$ and $\gamma = \pi/2$ and in Fig.13 is given the case of $|\eta| = 0.03, \eta' = 0.03$ and $\gamma = \pi/2$. In both cases, the pure CP violating effect and the fake CP violating effect due to the ordinary matter effect rapidly die out around 1.4 GeV, while the contribution of the FCNI effect survives significantly above this energy. Especially, the FCNI effect dominates the CP violating effect above 1 GeV for the case of $|\eta| = 0.10$ and $\eta' = 0.10$, as can be seen in Figs.12 and 14-15. In Fig.14 and Fig.15, the cases of $\Delta m^2_{31} > 0$ and $\Delta m^2_{31} < 0$ are taken, respectively, for $|\eta| = 0.10, \gamma = 3\pi/2$ and $\eta' = 0.10$. In Fig.16, the baseline is taken at $L = 730$ km for the energy range of $E = 0.5 - 2.5$ GeV for $|\eta| = 0.10, \gamma = \pi/2, \eta' = 0.10$ and $\Delta m^2_{31} > 0$. For this large baseline, both the ordinary and the FCNI matter effects become larger about 2-3 times than those for $L = 300$ km, and the FCNI effect dominates the CP violating effect above 1.8 GeV in the same way as for the case of $L = 300$ km. The oscillation pattern in the CP violating effect extends toward the larger

energy region as compared with that at $L = 300$ km due to the oscillation phase of $\Delta m^2_{31} L/(4E)$.

Next we see in Figs.17-18 the effects of NSNI in the CP violating effect in $\nu_\mu \to \nu_\mu$, which is the difference of $\nu_\mu \to \nu_\mu$ and $\bar{\nu_\mu} \to \bar{\nu_\mu}$ survival probabilities and shows only fake ones due to the matter effects. The long-dashed, short-dashed and dotted lines represent the ordinary, FCNI and FDNI matter effects, respectively, and the solid line does the total CP violating effect. In Fig.17 we give the CP violating effects in the energy range of $E = 0.3 - 2$ GeV at the baseline of $L = 300$ km for $|\eta| = 0.10, \gamma = \pi/2, \eta' = 0.10$, and $\Delta m^2_{31} > 0$. The ordinary matter effect is very small and the FCNI effect dominates above 0.8 GeV. In Fig.18, we give the CP violateing effect in $\nu_\mu \to \nu_\mu$ in the energy range of $E = 0.5 - 2.5$ GeV at the baseline of $L = 730$ km for $|\eta| = 0.10, \gamma = \pi/2, \eta' = 0.10$ and $\Delta m^2_{31} > 0$. Again, the ordinary matter effect and the FDNI effect are very small and the FCNI effect dominates.

IV Conclusions and discussions

In this paper we have studied the effect of non-standard neutrino matter interactions on the standard mass-induced oscillation probabilities and the CP violating effects. The non-standard interactions are introduced in the flavor-changing neutrino interaction (FCNI) and the flavor-diagonal one (FDNI) as sub-leading effects in the $\nu_\mu - \nu_\tau$ sector and $\nu_e - \nu_\mu$ sector in order to investigate their effects in $\nu_\mu \to \nu_\tau$ and $\nu_\mu \to \nu_e$ oscillations, respectively, at the baselines of $L = 730$ and 300 km. In $\nu_\mu \to \nu_\tau$ oscillation at $L = 730$ km, the FCNI contribution dominates and survives significantly above the neutrino energy 4 GeV, where all the others of pure CP violating effect, ordinary matter effect and FDNI contribution die out. Also in $\nu_\mu \to \nu_e$ oscillation at $L = 300$ km, the FCNI contribution dominates the CP violating effect above 1 GeV and survives significantly above 1.4 GeV,

where all the others of pure CP violating effect, ordinary matter effect and FDNI contribution die out.

These results show that the non-standard neutrino matter interations, especially the flavor-changing neutrino interaction, could be detected in the CP violating effect in neutrino oscillations at the neutrino energies where both the pure CP violating effect and the ordinary matter effect die out, for example, above 4 GeV in $\nu_\mu \to \nu_\tau$ oscillation at $L = 730$ km and around 1-2 GeV in $\nu_\mu \to \nu_e$ oscillation at $L = 300$ km. The FCNI effect might also be detected in the difference between $\nu_\mu \to \nu_\mu$ and $\bar{\nu_\mu} \to \bar{\nu_\mu}$ oscillation probabilities in 0.8-2 GeV at $L = 300$ km.

Appendix A: Oscillation probability with NSNI in $\nu_\mu - \nu_\tau$ sector

Here we present the oscillation probability of Eq.(8) with Eq.(19) taken in Eq.(18).

$$
\begin{aligned}
P \quad & (\nu_\alpha \to \nu_\beta; L) \\
= \quad & \delta_{\beta\alpha}\Big[\, 1 - 4\sin^2\left(\frac{\Delta m^2_{31}L}{4E}\right)\Big\{|U_{\alpha3}|^2[\, 1 - 2\frac{a}{\Delta m^2_{31}}(|U_{e3}|^2 - \delta_{\alpha e}) \\
& - 2\frac{\epsilon' b}{\Delta m^2_{31}}(|U_{\tau3}|^2 - \delta_{\alpha\tau})\,] - \frac{2}{\Delta m^2_{31}}\mathrm{Re}(\epsilon b U^*_{\mu3}U_{\tau3})(2|U_{\alpha3}|^2 - \delta_{\alpha\mu} - \delta_{\alpha\tau})\Big\} \\
& - 2\sin\left(\frac{\Delta m^2_{31}L}{2E}\right)|U_{\alpha3}|^2\Big\{\frac{aL}{2E}|U_{e3}|^2 + 2\frac{L}{2E}\mathrm{Re}(\epsilon b U^*_{\mu3}U_{\tau3}) + \frac{\epsilon' bL}{2E}|U_{\tau3}|^2\Big\}\,\Big] \\
& + 4\sin^2\left(\frac{\Delta m^2_{31}L}{4E}\right)\Big[\, |U_{\alpha3}|^2|U_{\beta3}|^2\{1 - 2\frac{a}{\Delta m^2_{31}}(2|U_{e3}|^2 - \delta_{\alpha e} - \delta_{\beta e}) \\
& - 2\frac{\epsilon' b}{\Delta m^2_{31}}(2|U_{\tau3}|^2 - \delta_{\alpha\tau} - \delta_{\beta\tau})\} - \frac{2}{\Delta m^2_{31}}\mathrm{Re}(\epsilon b U^*_{\mu3}U_{\tau3})\{4|U_{\alpha3}|^2|U_{\beta3}|^2 \\
& - |U_{\alpha3}|^2(\delta_{\beta\mu} + \delta_{\beta\tau}) - |U_{\beta3}|^2(\delta_{\alpha\mu} + \delta_{\alpha\tau})\}\,\Big] + 2\frac{\Delta m^2_{31}L}{2E}\sin\left(\frac{\Delta m^2_{31}L}{2E}\right) \\
& \times\Big[\, \frac{\Delta m^2_{21}}{\Delta m^2_{31}}\mathrm{Re}(U_{\beta3}U^*_{\beta2}U^*_{\alpha3}U_{\alpha2}) + \frac{a}{\Delta m^2_{31}}\{\delta_{\alpha e}\delta_{\beta e}|U_{e3}|^2 + |U_{\alpha3}|^2|U_{\beta3}|^2(2|U_{e3}|^2 \\
& - \delta_{\alpha e} - \delta_{\beta e})\} + \frac{\epsilon' b}{\Delta m^2_{31}}\{\delta_{\alpha\tau}\delta_{\beta\tau}|U_{\tau3}|^2 + |U_{\alpha3}|^2|U_{\beta3}|^2(2|U_{\tau3}|^2 - \delta_{\alpha\tau} - \delta_{\beta\tau})\} \\
& + \frac{1}{\Delta m^2_{31}}\mathrm{Re}(\epsilon b U^*_{\mu3}U_{\tau3})\{\delta_{\alpha\mu}\delta_{\beta\tau} + \delta_{\alpha\tau}\delta_{\beta\mu} + 4|U_{\alpha3}|^2|U_{\beta3}|^2 \\
& - |U_{\alpha3}|^2(\delta_{\beta\mu} + \delta_{\beta\tau}) - |U_{\beta3}|^2(\delta_{\alpha\mu} + \delta_{\alpha\tau})\}\,\Big] + 4\frac{\Delta m^2_{31}L}{2E}\sin^2\left(\frac{\Delta m^2_{31}L}{4E}\right) \\
& \times\Big[\, \frac{\Delta m^2_{21}}{\Delta m^2_{31}}\mathrm{Im}(U_{\beta3}U^*_{\beta2}U^*_{\alpha3}U_{\alpha2}) + \frac{1}{\Delta m^2_{31}}\mathrm{Im}(\epsilon b U^*_{\mu3}U_{\tau3})\{\delta_{\alpha\mu}\delta_{\beta\tau} - \delta_{\alpha\tau}\delta_{\beta\mu} \\
& + |U_{\alpha3}|^2(\delta_{\beta\mu} - \delta_{\beta\tau}) - |U_{\beta3}|^2(\delta_{\alpha\mu} - \delta_{\alpha\tau})\}\,\Big]. \qquad \text{(A1)}
\end{aligned}
$$

Appendix B: Oscillation probability with NSNI in $\nu_e - \nu_\mu$ sector

Here we present the oscillation probability of Eq.(8) with Eq.(26) taken in Eq.(18).

$$
\begin{aligned}
P \quad & (\nu_\alpha \to \nu_\beta; L) \\
= \quad & \delta_{\beta\alpha}\Big[\, 1 - 4\sin^2\left(\frac{\Delta m^2_{31}L}{4E}\right)\Big\{|U_{\alpha3}|^2[\, 1 - 2\frac{a}{\Delta m^2_{31}}(|U_{e3}|^2 - \delta_{\alpha e}) \\
& - 2\frac{\eta' b}{\Delta m^2_{31}}(|U_{\mu3}|^2 - \delta_{\alpha\mu})\,] - \frac{2}{\Delta m^2_{31}}\mathrm{Re}(\eta b U^*_{e3}U_{\mu3})(2|U_{\alpha3}|^2 - \delta_{\alpha\mu} - \delta_{\alpha e})\Big\} \\
& - 2\sin\left(\frac{\Delta m^2_{31}L}{2E}\right)|U_{\alpha3}|^2\Big\{\frac{aL}{2E}|U_{e3}|^2 + 2\frac{L}{2E}\mathrm{Re}(\eta b U^*_{e3}U_{\mu3}) + \frac{\eta' bL}{2E}|U_{\mu3}|^2\Big\}\,\Big] \\
& + 4\sin^2\left(\frac{\Delta m^2_{31}L}{4E}\right)\Big[\, |U_{\alpha3}|^2|U_{\beta3}|^2\{1 - 2\frac{a}{\Delta m^2_{31}}(2|U_{e3}|^2 - \delta_{\alpha e} - \delta_{\beta e}) \\
& - 2\frac{\eta' b}{\Delta m^2_{31}}(2|U_{\mu3}|^2 - \delta_{\alpha\mu} - \delta_{\beta\mu})\} - \frac{2}{\Delta m^2_{31}}\mathrm{Re}(\eta b U^*_{e3}U_{\mu3})\{4|U_{\alpha3}|^2|U_{\beta3}|^2 \\
& - |U_{\alpha3}|^2(\delta_{\beta e} + \delta_{\beta\mu}) - |U_{\beta3}|^2(\delta_{\alpha e} + \delta_{\alpha\mu})\}\,\Big] + 2\frac{\Delta m^2_{31}L}{2E}\sin\left(\frac{\Delta m^2_{31}L}{2E}\right) \\
& \times\Big[\, \frac{\Delta m^2_{21}}{\Delta m^2_{31}}\mathrm{Re}(U_{\beta3}U^*_{\beta2}U^*_{\alpha3}U_{\alpha2}) + \frac{a}{\Delta m^2_{31}}\{\delta_{\alpha e}\delta_{\beta e}|U_{e3}|^2 + |U_{\alpha3}|^2|U_{\beta3}|^2(2|U_{e3}|^2 \\
& - \delta_{\alpha e} - \delta_{\beta e})\} + \frac{\eta' b}{\Delta m^2_{31}}\{\delta_{\alpha\mu}\delta_{\beta\mu}|U_{\mu3}|^2 + |U_{\alpha3}|^2|U_{\beta3}|^2(2|U_{\mu3}|^2 - \delta_{\alpha\mu} - \delta_{\beta\mu})\} \\
& + \frac{1}{\Delta m^2_{31}}\mathrm{Re}(\eta b U^*_{e3}U_{\mu3})\{\delta_{\alpha e}\delta_{\beta\mu} + \delta_{\alpha\mu}\delta_{\beta e} + 4|U_{\alpha3}|^2|U_{\beta3}|^2 \\
& - |U_{\alpha3}|^2(\delta_{\beta e} + \delta_{\beta\mu}) - |U_{\beta3}|^2(\delta_{\alpha e} + \delta_{\alpha\mu})\}\,\Big] + 4\frac{\Delta m^2_{31}L}{2E}\sin^2\left(\frac{\Delta m^2_{31}L}{4E}\right) \\
& \times\Big[\, \frac{\Delta m^2_{21}}{\Delta m^2_{31}}\mathrm{Im}(U_{\beta3}U^*_{\beta2}U^*_{\alpha3}U_{\alpha2}) + \frac{1}{\Delta m^2_{31}}\mathrm{Im}(\eta b U^*_{e3}U_{\mu3})\{\delta_{\alpha e}\delta_{\beta\mu} - \delta_{\alpha\mu}\delta_{\beta e} \\
& + |U_{\alpha3}|^2(\delta_{\beta e} - \delta_{\beta\mu}) - |U_{\beta3}|^2(\delta_{\alpha e} - \delta_{\alpha\mu})\}\,\Big]. \qquad \text{(B1)}
\end{aligned}
$$

References

[1] Kamiokande Collaboration, K.S. Hirata et al., Phys. Lett. B **205**, 416(1988); Kamiokande Collaboration, Y. Fukuda et al., Phys. Lett. B **335**, 237(1994); IMB Collaboration, D. Casper et al., Phys. Rev. Lett. **66**, 2561(1991); IMB Collaboration, R. Becker-Szendy et al., Phys. Rev. D **46**, 3720(1992); Soudan2 Collaboration, W.W.M. Allison et al., Phys. Lett. B **391**, 491 (1997); **449**, 137 (1999); Super-Kamiokande Collaboration, Y. Fukuda et al., Phys. Lett. B **433**, 9 (1998); **436**, 33 (1998); Phys. Rev. Lett. **82**, 2644 (1999); MACRO Collaboration, M. Ambrosio et al., Phys. Lett. B **434**, 451 (1998); **478**, 5 (2000).

[2] Super-Kamiokande Collaboration, Y. Fukuda et al. Phys. Rev. Lett. **81**, 1562 (1998).

[3] Homestake Collaboration, B.T. Cleveland et al., Astrophys. J. **496**, 505 (1988); K. Lande et al., Nucl. Phys. B (Proc. Suppl.) **91**, 50 (2001); SAGE Collaboration, J.N. Abdurashitov et al., Phys. Rev. C **60**, 055801 (1999); GALLEX Collaboration, W. Hampel et al., Phys. Lett. B **447**, 127 (1999); GNO Collaboration, M. Altmann et al., Phys. Lett. B **490**, 16 (2000); Kamiokande Collaboration, Y. Fukuda et al., Phys. Rev. Lett. **77**, 1683 (1996); Super-Kamiokande Collaboration, Y. Fukuda et al., Phys. Rev. Lett. **81**, 1158 (1998); Erratum **81**, 4279 (1998); **82**, 1810 (1999); **82**, 2430 (1999); Super-Kamiokande Collaboration, S. Fukuda et al., Phys. Rev. Lett. **86**, 5651 (2001); SNO Collaboration, Q.R. Ahmad et al. , Phys. Rev. Lett. **87**, 071301 (2001); **89**, 011301 (2002); **89** 011302 (2002).

[4] J.N. Bahcall, P.I.Krastev, and A. Yu. Smirnov, Phys. Rev. D **58**, 096016 (1998); G. Fogli, E. Lisi, D. Montanino, and A. Palazzo, *ibid.* **62**, 013002 (2000); **64**, 093007 (2001); J.N. Bahcall, M.C. Gonzalez-Garcia, and C. Peña-

Garay, JHEP **0108**, 014 (2001); A. Bandyopadhyay, S. Choubey, S. Goswami, and K. Kar, Phys. Lett. B **519**, 83 (2001).

[5] S.P. Mikheyev and A.Yu. Smirnov, Sov. J. Nucl. Phys. **42**, 913 (1985); Nuovo Cimento **C9**, 17 (1986); L. Wolfenstein, Phys. Rev. D **17**, 2369 (1978).

[6] Z. Maki, M. Nakagawa, and S. Sakata, Prog. Theor. Phys. **28**, 870 (1962).

[7] M. Apollonio et al., Phys. Lett. B **420**, 397 (1998); **466**, 415 (1999).

[8] C. Athanassopoulos et al., Phys. Rev. Lett. **75**, 2650 (1995); **77**, 3082(1996); **81**, 1774(1998); R.L. Imlay (LSND Collaboration), in *ICHEP 2000*, Proceeindings of the 30th International Conference on High Energy Physics, Osaka, July 2000, eds. C.S. Lim and T. Yamanaka, p950.

[9] Wolfenstein [3]; L. Wolfenstein, Phys. Rev. D **20**, 2634 (1979).

[10] M.M. Guzzo, A. Masiero, and S.T. Petcov, Phys. Lett. B **260**, 154 (1991); E. Roulet, Phys. Rev. D **44**, 935 (1991).

[11] M.C. Gonzalez-Garcia, M.M. Guzzo, P.I. Krastev, H. Nunokawa, O.L.G. Peres, V. Pleitez, J.W.F. Valle, and R. Zukanovich Funchal, Phys. Rev. Lett. **82**, 3202 (1999).

[12] S. Bergmann, M.M. Guzzo, P.C. de Holanda, P.I. Krastev, and H. Nunokawa, Phys. Rev. D **62**, 073001 (2000).

[13] N. Fornengo, M. Maltoni, R. Tomàs Bayo, and J.W. Valle, Phys. Rev. D **65**, 013010 (2001).

[14] A.M. Gago, M.M. Guzzo, H. Nunokawa, W.J.C. Teves, and R. Zukanovich Funchal, Phys. Rev. D **64**, 073003 (2001).

[15] P. Huber and J.W.F. Valle, Phys. Lett. B **523**, 151 (2001).

[16] M.C. Gonzalez-Garcia, Y. Grossman, A. Gusso, and Y. Nir, Phys. Rev. D **64**, 096006 (2001).

[17] T. Ota, J. Sato, and N. Yamashita, Phys. Rev. D **65**, 093015 (2002).

[18] J. Arafune, M. Koike, and J. Sato, Phys. Rev. D **56**, 3093 (1997); **60**, 119905(E) (1999).

[19] Super-Kamiokande Collaboration, S. Fukuda et al. Phys. Rev. Lett. **86**, 5656 (2001).

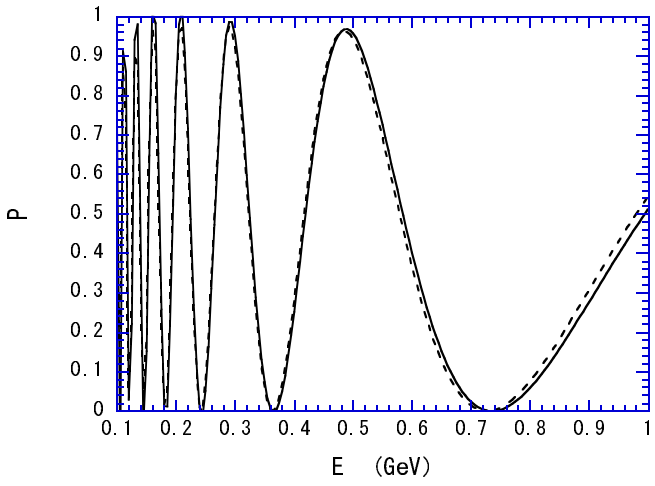

Figure 1: $\nu_\mu \to \nu_\tau$ oscillation probability for the neutrino energy range $E = 0.1-1$ GeV at the baseline of $L = 730$ km, with the NSNI in $\nu_\mu - \nu_\tau$ sector. The solid line is the one with all of the ordinary, FCNI and FDNI matter effects included for $|\epsilon| = 0.03, \epsilon' = 0.16, \phi = 0$ for the phase of ϵ, $\delta = \pi/2$ for the phase of $U, \Delta m^2_{21} = 5 \times 10^{-5}$ eV^2, and $\Delta m^2_{31} = 2.5 \times 10^{-3}$eV^2 (> 0). The dashed line is the one without any matter effects.

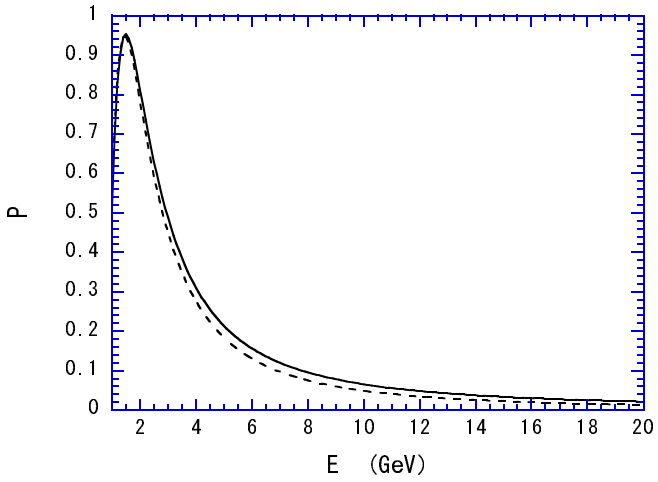

Figure 2: $\nu_\mu \to \nu_\tau$ oscillation probability for the neutrino energy range $E = 1 - 20$ GeV at $L = 730$ km with all of the ordinary, FCNI and FDNI matter effects included (solid line) and without any matter effects (dashed line). The parameter values are the same as in Fig.1.

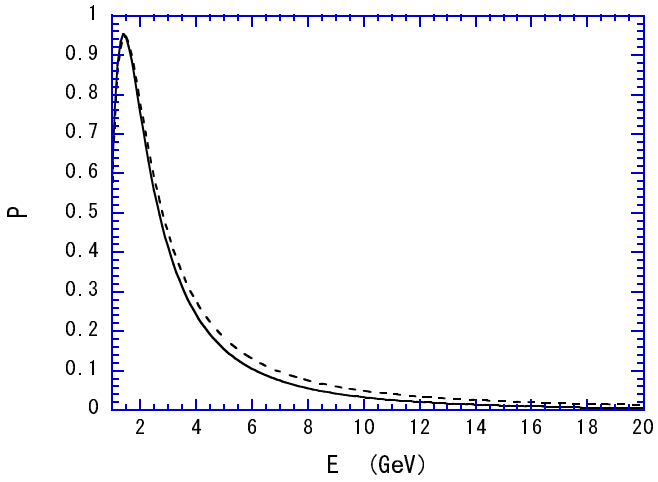

Figure 3: $\nu_\mu \to \nu_\tau$ oscillation probability for the neutrino energy range $E = 1 - 20$ GeV at $L = 730$ km with all of the ordinary, FCNI and FDNI matter effects included (solid line) and without any matter effects (dashed line). The parameter values are the same as in Fig.1 except for $\phi = \pi$.

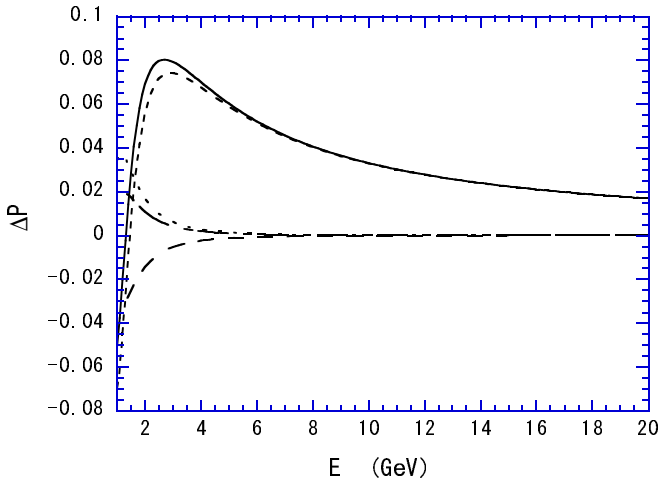

Figure 4: The CP violating effect in $\nu_\mu \to \nu_\tau$ oscillation for the neutrino energy range $E = 1 - 20$ GeV at $L = 730$ km, with the NSNI in $\nu_\mu - \nu_\tau$ sector. The dash-dotted line is the pure CP violating effect. The long-dashed, short-dashed and dotted lines are the fake CP violating effects due to the ordinary, FCNI and FDNI matter effects, respectively. The solid line is the total CP violating effect with the pure and fake ones. The parameter values are $|\epsilon| = 0.03, \epsilon' = 0.16, \phi = 0, s_{12} = 0.541, s_{23} = 0.742, s_{13} = 0.16, \delta = \pi/2, \Delta m^2_{21} = 5 \times 10^{-5}$ eV^2, and $\Delta m^2_{31} = 2.5 \times 10^{-3}$eV^2 (> 0).

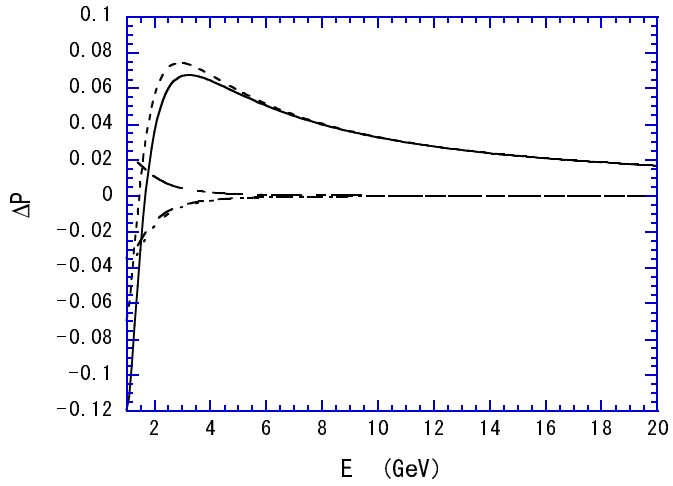

Figure 5: The CP violating effect in $\nu_\mu \to \nu_\tau$ oscillation at $L = 730$ km with the same parameter values as in Fig.4 except for $\epsilon' = -0.16$. The lines represent the same ones as in Fig.4. The FDNI contribution changes the sign as compared with the one in Fig.4.

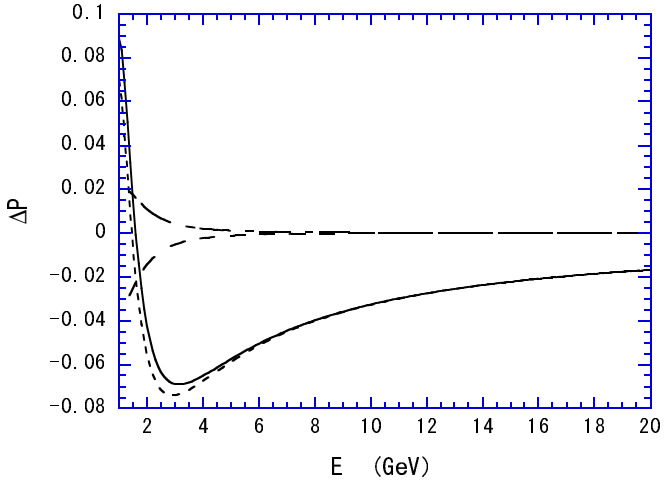

Figure 6: The CP violating effect in $\nu_\mu \to \nu_\tau$ oscillation at $L = 730$ km with the same parameter values as in Fig.4 except for $\phi = \pi$. The lines represent the same ones as in Fig.4 except for the line of FDNI contribution omitted.

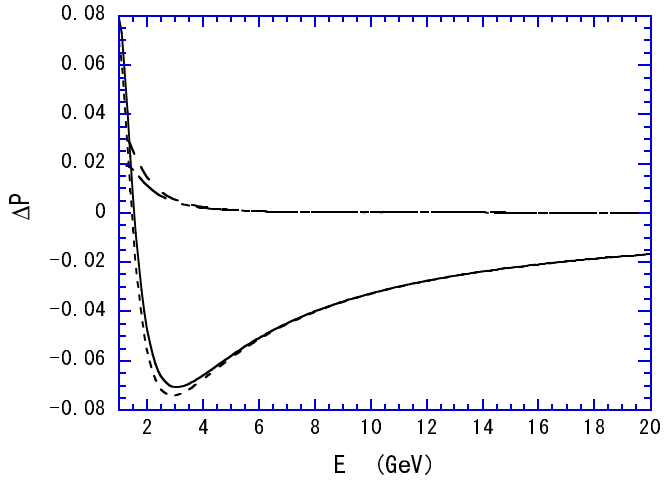

Figure 7: The CP violating effect in $\nu_\mu \to \nu_\tau$ oscillation at $L = 730$ km with the same parameter values as in Fig.4 except for $\Delta m^2_{31} < 0$. The lines represent the same ones as in Fig.4 except for the line of FDNI contribution omitted.

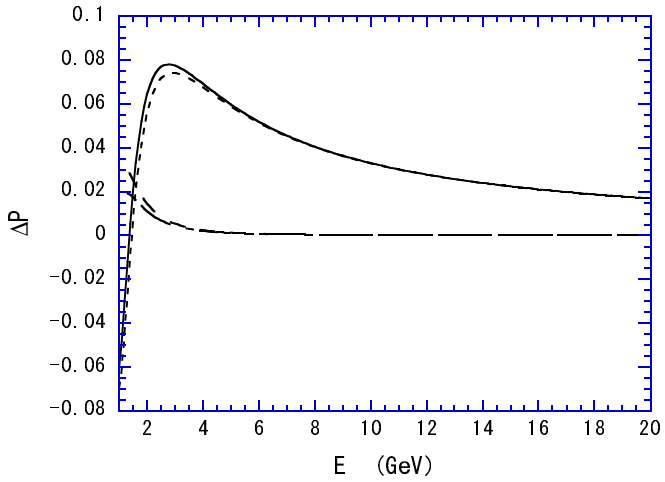

Figure 8: The CP violating effect in $\nu_\mu \to \nu_\tau$ oscillation at $L = 730$ km with the same parameter values as in Fig.4 except for $\phi = \pi$ and $\Delta m^2_{31} < 0$. The lines represent the same ones as in Fig.4 except for the line of FDNI contribution omitted.

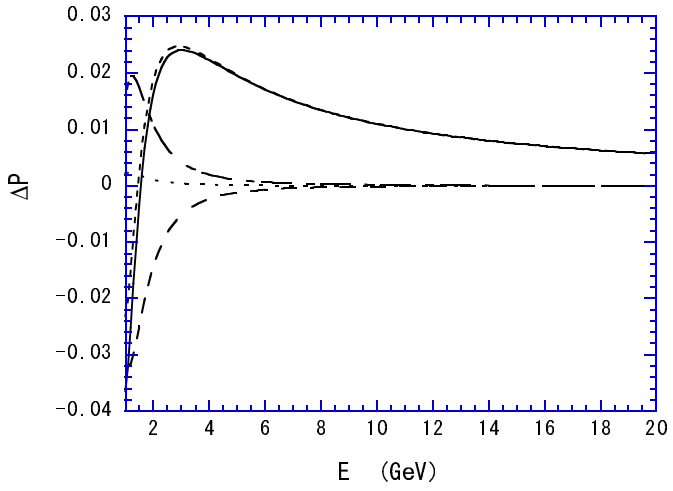

Figure 9: The CP violating effect in $\nu_\mu \to \nu_\tau$ oscillation at $L = 730$ km with the same parameter values as in Fig.4 except for $|\epsilon| = 0.01$ and $\epsilon' = 0.01$. The lines represent the same ones as in Fig.4.

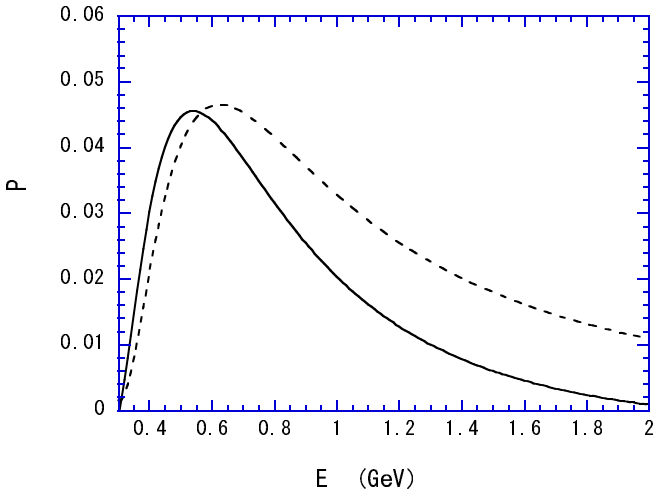

Figure 10: $\nu_\mu \to \nu_e$ oscillation probability for the neutrino energy range $E = 0.3{-}2$ GeV at the baseline of $L = 300$ km, with the NSNI in $\nu_e - \nu_\mu$ sector. The solid line is the one with all of the ordinary, FCNI and FDNI matter effects included for $|\eta| = 0.10, \eta' = 0.10, \gamma = \pi/2$ for the phase of η, $\delta = \pi/2$ for the phase of $U, \Delta m^2_{21} = 5 \times 10^{-5}$ eV^2, and $\Delta m^2_{31} = 2.5 \times 10^{-3}$eV^2 (> 0). The dashed line is the one without any matter effects.

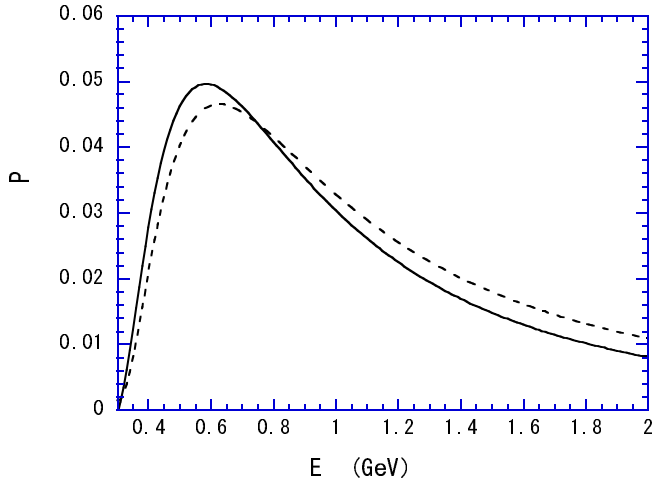

Figure 11: $\nu_\mu \to \nu_e$ oscillation probability at $L = 300$ km with all of the ordinary, FCNI and FDNI matter effects included (solid line) and without any matter effects (dashed line). The parameter values are the same as in Fig.10 except for $|\eta| = 0.03$ and $\eta' = 0.03$.

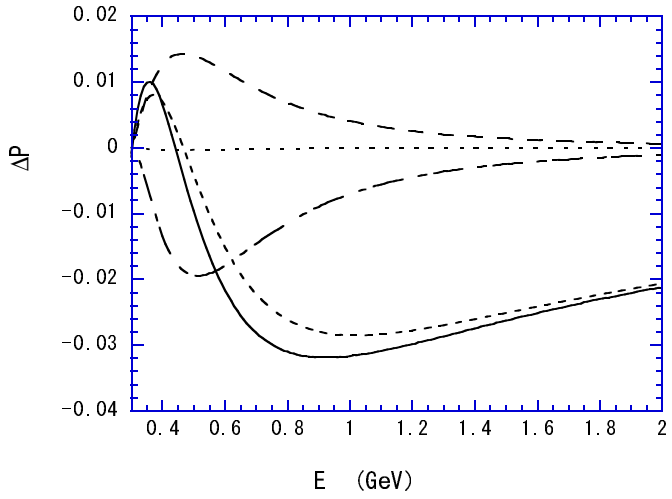

Figure 12: The CP violating effect in $\nu_\mu \to \nu_e$ oscillation for the neutrino energy range $E = 0.3 - 2$ GeV at $L = 300$ km, with the NSNI in $\nu_e - \nu_\mu$ sector. The dash-dotted line is the pure CP violating effect. The long-dashed, short-dashed and dotted lines are the fake CP violating effects due to the ordinary, FCNI and FDNI matter effects, respectively. The solid line is the total CP violating effect with the pure and fake ones. The parameter values are $|\eta| = 0.10, \eta' = 0.10, \gamma = \pi/2, s_{12} = 0.541, s_{23} = 0.742, s_{13} = 0.16, \delta = \pi/2, \Delta m^2_{21} = 5 \times 10^{-5}$ eV^2, and $\Delta m^2_{31} = 2.5 \times 10^{-3}$eV^2 (> 0).

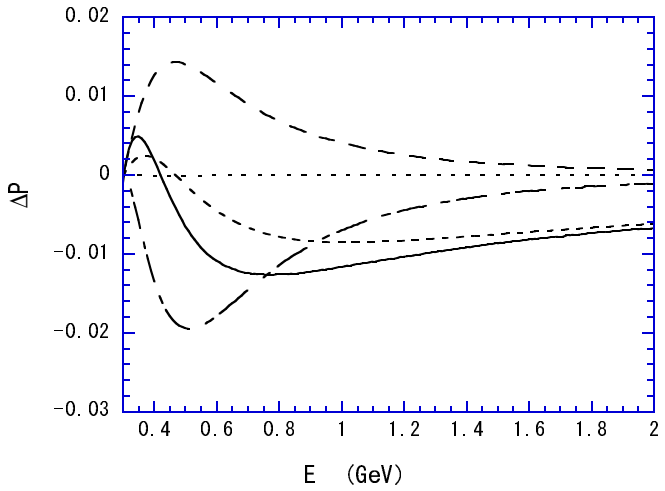

Figure 13: The CP violating effect in $\nu_\mu \to \nu_e$ oscillation at $L = 300$ km with the same parameter values as in Fig.12 except for $|\eta| = 0.03$ and $\eta' = 0.03$. The lines represent the same ones as in Fig.12.

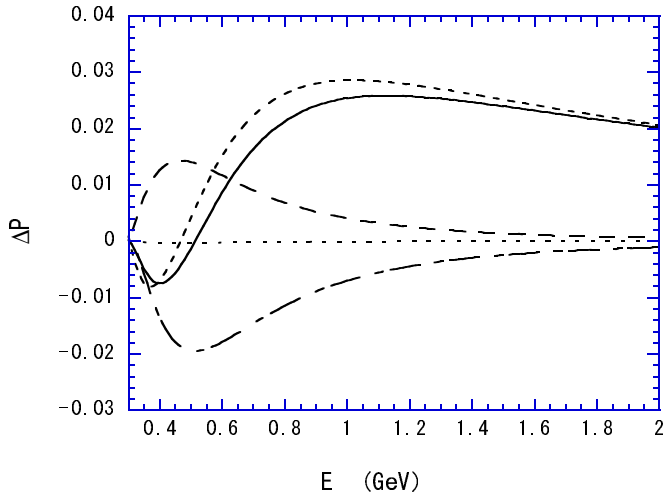

Figure 14: The CP violating effect in $\nu_\mu \to \nu_e$ oscillation at $L = 300$ km with the same parameter values as in Fig.12 except for $\gamma = 3\pi/2$. The lines represent the same ones as in Fig.12.

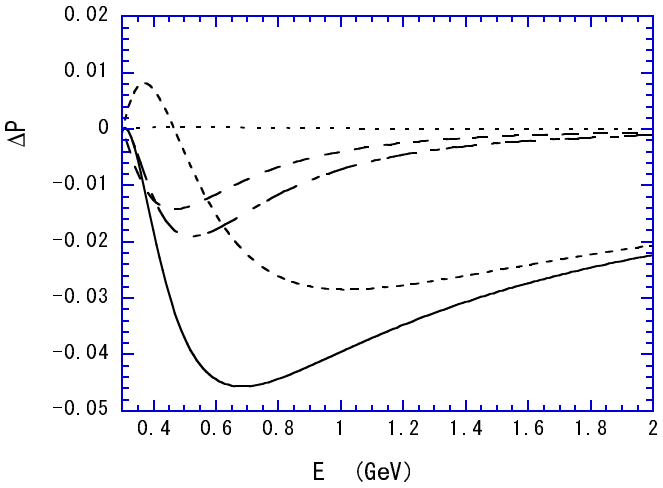

Figure 15: The CP violating effect in $\nu_\mu \to \nu_e$ oscillation at $L = 300$ km with the same parameter values as in Fig.12 except for $\gamma = 3\pi/2$ and $\Delta m^2_{31} < 0$. The lines represent the same ones as in Fig.12.

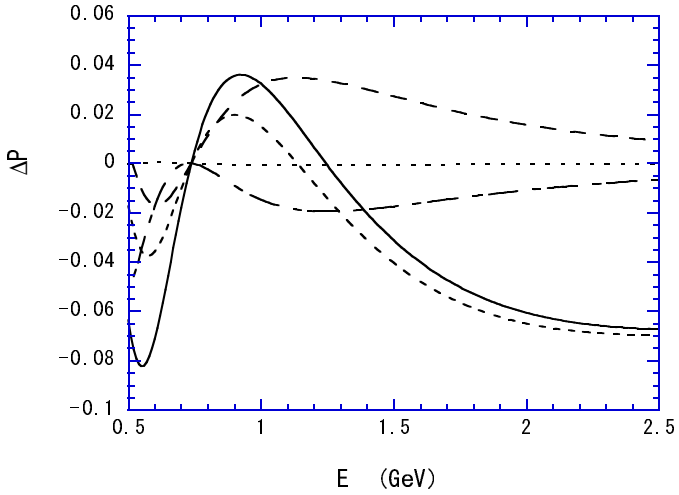

Figure 16: The CP violating effect in $\nu_\mu \to \nu_e$ oscillation for the neutrino energy range $E = 0.5 - 2.5$ GeV at $L = 730$ km with the same parameter values as in Fig.12. The lines represent the same ones as in Fig.12. The only change from Fig.12 is the baseline length.

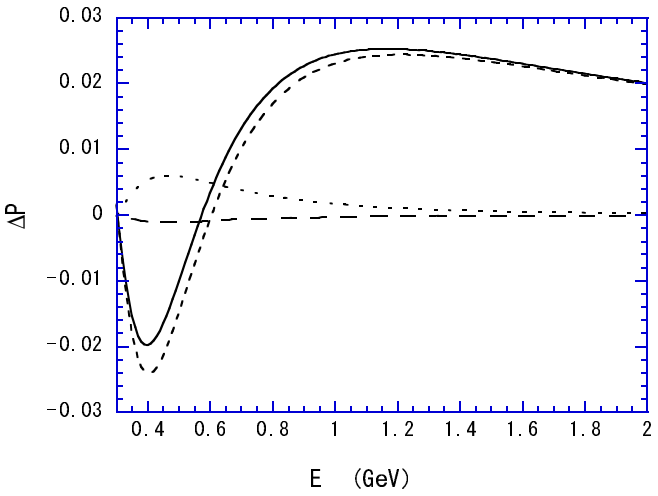

Figure 17: The CP violating effect in $\nu_\mu \to \nu_\mu$ for the neutrino energy range $E = 0.3 - 2$ GeV at $L = 300$ km, with the NSNI in $\nu_e - \nu_\mu$ sector. The long-dashed, short-dashed and dotted lines are the fake CP violating effects due to the ordinary, FCNI and FDNI matter effects, respectively. The solid line is the total CP violating effect with these three matter effects. The parameter values are $|\eta| = 0.10, \eta' = 0.10, \gamma = \pi/2, s_{12} = 0.541, s_{23} = 0.742, s_{13} = 0.16, \delta = \pi/2, \Delta m^2_{21} = 5 \times 10^{-5}$ eV^2, and $\Delta m^2_{31} = 2.5 \times 10^{-3}$eV^2 (> 0).

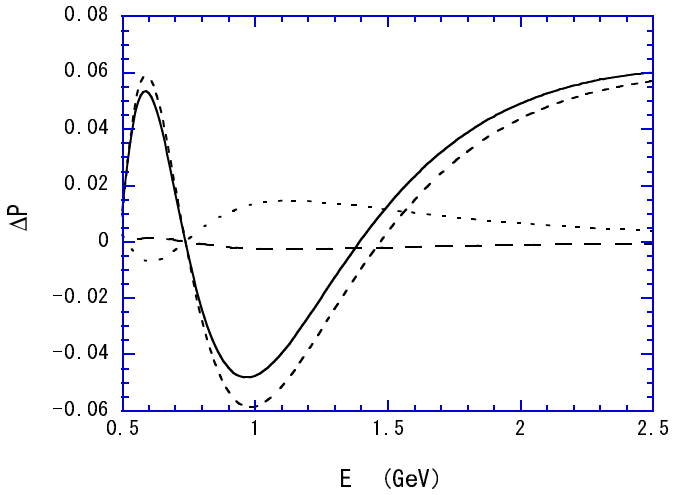

Figure 18: The CP violating effect in $\nu_\mu \to \nu_\mu$ oscillation for the neutrino energy range $E = 0.5 - 2.5$ GeV at $L = 730$ km with the same parameter values as in Fig.17. The lines represent the same ones as in Fig.17. The only change from Fig.17 is the baseline length.